crystals

MDPI

Article

Polymorphisms in $M^{2+}AlF_5(H_2O)_7$ (M^{2+} = Fe^{2+}, Co^{2+}, or Ni^{2+}): Syntheses, Crystal Structures, and Characterization of New Mixed Metal Fluoride Hydrates

Jun Min Seo [1], Hongil Jo [2], Myung Ho Choi [2], Kang Min Ok [2], Hong Young Chang [3] and Sun Woo Kim [1,*]

[1] Department of Chemistry Education, Chosun University, Gwangju 61452, Republic of Korea
[2] Department of Chemistry, Sogang University, Seoul 04107, Republic of Korea; hongil.jo@liverpool.ac.uk (H.J.); kmok@sogang.ac.kr (K.M.O.)
[3] Department of Computer, Mathematical and Physical Sciences (CMPS), Sul Ross State University, Alpine, TX 79832, USA; hong.young.chang@sulross.edu
* Correspondence: swookim@chosun.ac.kr

Abstract: Three new mixed metal fluoride hydrates, $M^{2+}AlF_5(H_2O)_7$ (M^{2+} = Fe^{2+}, Co^{2+}, or Ni^{2+}), were synthesized and characterized. The crystals of $M^{2+}AlF_5(H_2O)_7$ were obtained using a hydrothermal method with a CF_3COOH aqueous solution. The crystal structures displayed polymorphisms in $C2/m$ (No. 12) or P-1 (No. 2) space groups, depending on temperature variations. The observed polymorphisms in $M^{2+}AlF_5(H_2O)_7$ are associated with changes in the bonding environment of $[M(H_2O)_6]^{2+}$ and $[AlF_5(H_2O)]^{2-}$ octahedra, along with changes in hydrogen bonds and unit cell volumes. Infrared spectra and thermogravimetric analyses confirmed the presence of water molecules. The ultraviolet–visible spectra of $M^{2+}AlF_5(H_2O)_7$ revealed distinctive absorption bands dependent on the $[M(H_2O)_6]^{2+}$ complex. This work provides a detailed account of the synthetic procedure, crystal structures, and spectroscopic characterization of $M^{2+}AlF_5(H_2O)_7$.

Keywords: polymorphisms; fluorides; hydrothermal; hydrogen bonding; mixed metal

check for updates

Citation: Seo, J.M.; Jo, H.; Choi, M.H.; Ok, K.M.; Chang, H.Y.; Kim, S.W. Polymorphisms in $M^{2+}AlF_5(H_2O)_7$ (M^{2+} = Fe^{2+}, Co^{2+}, or Ni^{2+}): Syntheses, Crystal Structures, and Characterization of New Mixed Metal Fluoride Hydrates. *Crystals* **2024**, *14*, 197. https://doi.org/10.3390/cryst14020197

Academic Editor: Waldemar Maniukiewicz

Received: 22 January 2024
Revised: 14 February 2024
Accepted: 16 February 2024
Published: 17 February 2024

Copyright: © 2024 by the authors. Licensee MDPI, Basel, Switzerland. This article is an open access article distributed under the terms and conditions of the Creative Commons Attribution (CC BY) license (https://creativecommons.org/licenses/by/4.0/).

1. Introduction

Mixed metal fluoride materials have captured considerable attention due to their varied and intriguing physical properties [1], including their multiferroic behavior ($BaMnF_4$ [2–4], $BaCoF_4$ [5–7], $BaNiF_4$ [8,9], $K_3Fe_5F_{15}$ [10–12], $K_3Cr_2Fe_3F_{15}$ [13,14], and $Pb_5Cr_3F_{19}$ [15,16]), non-linear optical (NLO) behavior ($BaMgF_4$ [17,18], KNa_2ZrF_7 [19], and $CsNaTaF_7$ [20]), and luminescent features (Yb^{3+}/Er^{3+}-co-doped $NaYF_4$ [21], Mn^{4+}-doped K_2LiAlF_6 [22], and Tb^{3+}-doped $Na_5Lu_9F_{32}$ [23]). Despite the allure of these properties, research on mixed metal fluoride materials has been limited compared to oxide materials, primarily due to challenges in their synthesis.

Traditionally, solid-state reactions for the synthesis of fluoride materials have relied on HF, F_2, and CF_4 gases as fluorination sources to prevent hydrolysis into oxides [24]. However, the use of these gases is inherently hazardous and toxic, and it requires meticulous precautions for safe handling. An alternative approach for fluoride material synthesis involves hydrothermal or solvothermal methods. Nevertheless, these methods introduce HF to regulate the reaction acidity, posing difficulties due to its toxicity and its tendency to dissolve glass materials in synthetic experiments. Furthermore, many fluoride materials lack well-defined crystal structures and comprehensive characterizations. Therefore, there is a pressing need for innovative synthetic methods and strategies to facilitate the creation and in-depth study of these materials, unraveling their unique physical properties.

Kim et al. previously presented an innovative synthetic method for making complex fluoride materials. Instead of utilizing an aqueous HF solution via the hydrothermal route, they employed a CF_3COOH aqueous solution, resulting in materials such as $BaMF_4$

(M = Mg, Mn, Co, Ni, and Zn) [25], $RbFe_2F_6$ [26], and $K_4Fe_3F_{12}$ [27]. Consequently, this method opens the door for the synthesis of various new mixed metal fluoride materials.

In previous studies, mixed metal fluorides hydrates, denoted as $M^{2+}M'^{3+}F_5(H_2O)_7$ (M = Mn^{2+}, Co^{2+}, Ni^{2+}, Cu^{2+}, or Zn^{2+}; M' = Al^{3+}, Cr^{3+}, Mn^{3+}, Fe^{3+}, Ga^{3+}, or In^{3+}) have been reported, with crystal structures identified as *P*-1 (No. 2), *C*2/*m* (No. 12), or *C*2/*c* (No. 15) space groups depending on their chemical compositions (See Table 1) [28–31]. Notably, the crystal structure of $NiFeF_5(H_2O)_7$ exhibits polymorphisms (*P*-1 or *C*2/*c*) dependent on the temperature [30]. Furthermore, the crystal structure of $NiGaF_5(H_2O)_7$ also displays polymorphisms (*P*-1 or *C*2/*m*) contingent on synthetic conditions [31]. These findings suggest that the polymorphic characteristics of the crystal structures in $M^{2+}M'^{3+}F_5(H_2O)_7$ also may be influenced by specific chemical compositions and/or synthetic conditions. Building on these insights, we aim to further explore compositional modifications and controlled synthetic conditions of $M^{2+}M'^{3+}F_5(H_2O)_7$ to uncover novel crystal structures, including polymorphisms with intriguing physical properties.

Table 1. Crystallographic parameters of $M^{2+}M'^{3+}F_5(H_2O)_7$ (M^{2+} = Mn^{2+}, Fe^{2+}, Co^{2+}, Ni^{2+}, Cu^{2+}, or Zn^{2+}; M'^{3+} = Al^{3+}, Cr^{3+}, Mn^{3+}, Fe^{3+}, Ga^{3+}, or In^{3+}).

Compound	Space Group, T	Lattice Parameter (Å)	V(Å^3)	Reference
$CoAlF_5(H_2O)_7$	*C*2/m, 296 K	*a* =10.917(7), *b* = 13.863(14), *c* = 6.525(5), β = 100.30(6)°	971.60	[28]
$MnFeF_5(H_2O)_7$	*C*2/c, 296 K	*a* = 11.182(3), *b* = 14.168(4), *c* = 13.264(3), β = 100.51(2)°	2066.12	[28]
$CuInF_5(H_2O)_7$	*P*-1, 100 K	*a* = 6.5659(5), *b* = 8.8631(6), *c* = 9.1548(6), α = 103.16(1)°, β = 97.66(1)°, γ = 97.31(1)°	507.24(6)	[29]
$ZnGaF_5(H_2O)_7$	*P*-1, 296 K	*a* = 6.5659(5), *b* = 8.8631(6), *c* = 9.1548(6), α = 103.16(1)°, β = 97.66(1)°, γ = 97.31(1)°	486.18(3)	[29]
$NiMnF_5(H_2O)_7$	*P*-1, 100(2) K	*a* = 6.4149(2), *b* = 8.9609(2), *c* = 8.9609(2), α = 104.1985(10)°, β = 95.9379(10)°, γ = 96.6946(10)°	491.22(2)	[30]
$NiCrF_5(H_2O)_7$	*P*-1, 100(2) K	*a* = 6.4661(4), *b* = 8.6504(5), *c* = 8.8679(5), α = 104.6606(19)°, β = 96.584(2)°, γ = 94.423(2)°	473.67(5)	[30]
$NiFeF_5(H_2O)_7$	*C*2/c, 301(2) K	*a* = 10.9229(3), *b* = 13.9060(3), *c* = 13.0252(4), β = 100.2400(10)°	1946.93(9)	[30]
	P-1, 100(2) K	*a* = 6.4783(3), *b* = 8.699(3), *c* = 8.9131(4), α = 104.5130(10)°, β = 96.9280(10)°, γ = 94.5090(10)°	479.31(4)	[30]
$CoInF_5(H_2O)_7$	*C*2/c, 300(2) K	*a* = 11.1238(4), *b* = 14.2361(5), *c* = 13.3064(5), β = 100.7280(14)°	2070.37(13)	[31]
$NiInF_5(H_2O)_7$	*P*-1, 300(2) K	*a* = 6.61530(10), *b* = 8.9621(2), *c* = 8.9961(2), α = 102.9620(10)°, β = 98.3470(10)°, γ = 96.3110(10)°	508.609(18)	[31]
$NiGaF_5(H_2O)_7$	*C*2/m, 300(2) K	*a* =10.8563(4), *b* = 13.8331(5), *c* = 6.4968(2), β = 99.9610(10)°	960.96(6)	[31]
	P-1, 300(2) K	*a* = 6.4800(2), *b* = 8.6957(3), *c* = 8.8694(3), α = 103.9584(12)°, β = 96.8177(13)°, γ = 95.1076(12)°	477.98(3)	[31]

Table 1. *Cont.*

Compound	Space Group, T	Lattice Parameter (Å)	V(Å^3)	Reference
$FeAlF_5(H_2O)_7$	*C*2/m, 300(2) K	*a* = 10.9189(7), *b* = 13.8020(7), *c* = 6.5210(4), β = 100.154(2)°	967.26(10)	This work
	P-1, 100(2) K	*a* = 6.4864(9), *b* = 8.7190(11), *c* = 8.7917(11), α = 103.934(3)°, β = 96.364(3)°, γ = 95.400(3)°	476.05(11)	
$CoAlF_5(H_2O)_7$	*C*2/m, 300(2) K	*a* = 10.8749, *b* = 13.7822(16), *c* = 6.4894(8), β = 100.397(5)°	956.7(2)	This work
	P-1, 100(2) K	*a* = 6.4434(5), *b* = 8.6691(6), *c* = 8.8031(6), α = 104.019(2)°, β = 96.749(2)°, γ = 95.254(2)°	470.08(6)	
$NiAlF_5(H_2O)_7$	*C*2/m, 296(2) K	*a* = 10.7880(4), *b* = 13.6952(4), *c* = 6.4554(2), β = 100.1507(14)°	938.82(6)	This work
	P-1, 101(2) K	*a* = 6.4022(6), *b* = 8.5874(7), *c* = 8.7691(7), α = 104.255(3)°, β = 96.638(3)°, γ = 94.816(3)°	460.96(7)	

In the current study, utilizing a hydrothermal method with a CF_3COOH aqueous solution, we delve into the detailed syntheses, crystal structures at both room temperature and 100 K, and characterization of three noble mixed metal fluorides hydrates, specifically $M^{2+}AlF_5(H_2O)_7$, where M represents Fe, Co, or Ni. While the room temperature crystal structure of $CoAlF_5(H_2O)_7$ has been previously reported [28], its crystal structure at 100 K has not been explored.

2. Materials and Methods

The following reagents were used without purification: FeF_2 (Alfa Aesar, Haverhill, MA, USA, 99.5%), CoF_2 (Alfa Aesar, Haverhill, MA, USA, 98%), NiF_2 (Alfa Aesar, Haverhill, MA, USA, 97%), AlF_3 (Alfa Aesar, Haverhill, MA, USA, 99.5%), and CF_3COOH (Alfa Aesar, Haverhill, MA, USA, 99%).

$M^{2+}AlF_5(H_2O)_7$ (M^{2+} = Fe^{2+}, Co^{2+}, or Ni^{2+}) were synthesized using a mild hydrothermal method using aqueous CF_3COOH solution (see Figure 1).

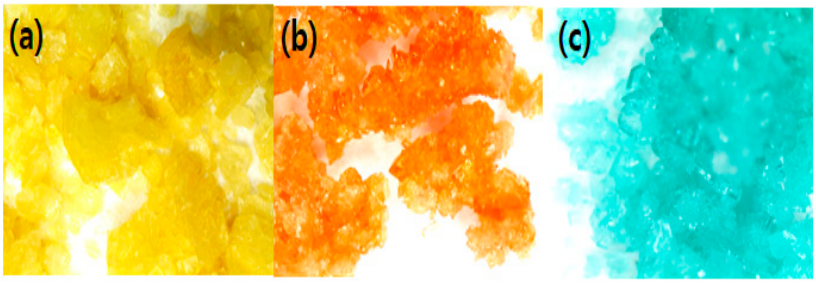


Figure 1. Photographs of crystals of $M^{2+}AlF_5(H_2O)_7$ (M^{2+} = Fe^{2+}, Co^{2+}, or Ni^{2+}): (**a**) $FeAlF_5(H_2O)_7$, (**b**) $CoAlF_5(H_2O)_7$, and (**c**) $NiAlF_5(H_2O)_7$.

Crystals of $FeAlF_5(H_2O)_7$ were grown by mixing 0.1473 g (1.57 mmol) of FeF_2, 0.1318 g (1.57 mmol) of AlF_3, 3 mL of CF_3COOH (39 mmol), and 5 mL of H_2O. The resultant solution was placed in a 23 mL Teflon-lined stainless autoclave that was subsequently closed. The autoclave was gradually heated to 230 °C, held for 24 h, and cooled slowly to room temperature at a rate of 6 °C/h. The mother liquor was decanted from the products, then the products were recovered via filtration and washed with distilled water and acetone. Slightly yellowish-colored block-shaped crystals, the only product of the reaction, were recovered with a ~50% yield based on AlF_3. The powder X-ray diffraction pattern of the

synthesized phase was in good agreement with the generated pattern from the single crystal data (see Supporting Information, Figure S1).

Crystals of $CoAlF_5(H_2O)_7$ were grown by mixing 0.1521 g (1.57 mmol) of CoF_2, 0.1318 g (1.57 mmol) of AlF_3, 3 mL of CF_3COOH (39 mmol), and 5 mL of H_2O. The resultant solution was placed in a 23 mL Teflon-lined stainless autoclave that was subsequently closed. The autoclave was gradually heated to 230 °C, held for 24 h, and cooled slowly to room temperature at a rate of 6 °C/h. The mother liquor was decanted from the products, then the products were recovered via filtration and washed with distilled water and acetone. Orange-colored block-shaped crystals, the only product of the reaction, were recovered with an ~80% yield based on AlF_3. The powder X-ray diffraction pattern of the synthesized phase was in good agreement with the generated pattern from the single crystal data (see Supporting Information, Figure S1).

Crystals of $NiAlF_5(H_2O)_7$ were grown by mixing 0.1518 g (1.57 mmol) of NiF_2, 0.1318 g (1.57 mmol) of AlF_3, 3 mL of CF_3COOH (39 mmol), and 5 mL of H_2O. The resultant solution was placed in a 23 mL Teflon-lined stainless autoclave that was subsequently closed. The autoclave was gradually heated to 230 °C, held for 24 h, and cooled slowly to room temperature at a rate of 6 °C/h. The mother liquor was decanted from the products, then the products were recovered via filtration and washed with distilled water and acetone. Blue–green-colored block-shaped crystals, the only product of the reaction, were recovered with an ~80% yield based on AlF_3. The powder X-ray diffraction pattern of the synthesized phase was in good agreement with the generated pattern from the single crystal data (see Supporting Information, Figure S1).

Single crystal X-ray diffraction (SCXRD) data for $M^{2+}AlF_5(H_2O)_7$ (M^{2+} = Fe^{2+}, Co^{2+}, or Ni^{2+}) were collected using a Bruker D8 QUEST diffractometer with graphite-monochromated Mo Kα radiation (λ = 0.71073 Å) and a PHOTON-II CPAD detector at room temperature and 100 K, respectively. For data collection, a slightly yellowish-colored block-shaped crystal of $FeAlF_5(H_2O)_7$ (0.051 mm × 0.154 mm × 0.212 mm), an orange-colored block-shaped crystal of $CoAlF_5(H_2O)_7$ (0.051 mm × 0.154 mm × 0.212 mm), and a blue–green-colored block-shaped crystal of $NiAlF_5(H_2O)_7$ (0.088 mm × 0.150 mm × 0.151 mm) were selected and mounted on a glass fiber. The data were integrated using the SAINT program [32] with the intensities corrected for Lorentz, polarization, and air absorption. Multiple scans were used for the absorption correction across the hemisphere of the data. The crystallographic space group for the structures of $M^{2+}AlF_5(H_2O)_7$ (M^{2+} = Fe^{2+}, Co^{2+}, or Ni^{2+}) under ~100 K or room temperature were determined as *P*-1 (No. 2) and *C*2/*m* (No. 12), respectively. The systematic forbidden reflections ($h + k = 2n + 1$) attributable to the *C*-centered cell of the *C*2/*m* space group were observed as the reflection conditions of the *P*-1 space group. Thus, two space groups, *P*-1 and *C*2/*m*, were clearly distinguished [33]. The structures were solved via the direct method (SHELXS-2014) [34,35], and all the atomic positions are thermal parameters were refined using the program SHELXL (2019/3) [34,35]. Notably, the crystal structures of $M^{2+}AlF_5(H_2O)_7$ (M^{2+} = Fe^{2+}, Co^{2+}, or Ni^{2+}) at 100 K were refined as pseudo-merohedral twins. The data were converged for $I > 2\sigma(I)$. All calculations were performed using the WINGX-98 crystallographic software package [36]. Relevant crystallographic data and selected bond distances for $M^{2+}AlF_5(H_2O)_7$ (M^{2+} = Fe^{2+}, Co^{2+}, or Ni^{2+}) are given in Tables 2–4. Further details are available in the Supporting Information, specifically, in Tables S1 and S2. Additionally, the local coordination environments of $M^{2+}AlF_5(H_2O)_7$ (M^{2+} = Fe^{2+}, Co^{2+}, or Ni^{2+}) are illustrated in the Supporting Information, Figure S2. The structural figures for $M^{2+}AlF_5(H_2O)_7$ (M^{2+} = Fe^{2+}, Co^{2+}, or Ni^{2+}) were drawn using the VESTA crystal structure drawing package [37].

Table 2. Crystallographic data for $M^{2+}AlF_5(H_2O)_7$ (M^{2+} = Fe^{2+}, Co^{2+}, or Ni^{2+}).

	$FeAlF_5(H_2O)_7$		**$CoAlF_5(H_2O)_7$**		**$NiAlF_5(H_2O)_7$**	
F.W.	303.94		307.02		306.80	
T(K)	300	100(2)	300(2)	100(2)	296(2)	101(2)
Crystal system	Monoclinic	Triclinic	Monoclinic	Triclinic	Monoclinic	Triclinic
Space group	*C*2/*m* (No. 12)	*P*-1 (No. 2)	*C*2/*m* (No. 12)	*P*-1 (No. 2)	*C*2/*m* (No. 12)	*P*-1 (No. 2)
a (Å)	10.9180(7)	6.4864(9)	10.8749(16)	6.4434(5)	10.7880(4)	6.4022(6)
b (Å)	13.8020(7)	8.7190(11)	13.7822(16)	8.6691(6)	13.6952(4)	8.5874(7)
c (Å)	6.5210(4)	8.7917(11)	6.4894(8)	8.8031(6)	6.4554(2)	8.7691(7)
Angle (deg)	β = 100.154(2)	α = 103.834(3) β = 96.364(3) γ = 95.400(3)	β = 100.397(5)	α = 104.019(2) β = 96.749(2) γ = 95.254(2)	β = 100.1507(14)	α = 104.255(3) β = 96.638(3) γ = 94.816(3)
V (Å)^3	967.26(10)	476.05(11)	956.7(2)	470.08(6)	938.82(6)	460.96(7)
Z	4	2	4	2	4	2
ρ_{cald} (g/cm^3)	2.087	2.120	2.132	2.169	2.171	2.210
μ (mm^{-1})	1.742	1.770	1.979	2.014	2.255	2.296
$2\theta_{max}$(deg)	56.84	56.64	66.18	56.82	56.66	56.66
R(int)	0.0487	0.0336	0.0350	0.0424	0.0214	0.0435
GOF	1.085	1.129	1.111	1.148	1.116	1.121
$R(F)$ [a]	0.0424	0.0425	0.0434	0.0329	0.0407	0.0512
$R_w(F_o^2)$ [b]	0.0997	0.1133	0.1031	0.0743	0.0945	0.1408

[a] $R(F) = \Sigma||F_o| - |F_c||/\Sigma|F_o|$, [b] $R_w(F_o^2) = [\Sigma w(F_o^2 - F_c^2)^2/\Sigma w(F_o^2)^2]^{1/2}$.

Table 3. Selected bond distances for $M^{2+}AlF_5(H_2O)_7$ (M^{2+} = Fe^{2+}, Co^{2+}, or Ni^{2+}) at RT.

Bond	**Distance (Å)**	**Bond**	**Distance (Å)**
	$FeAlF_5(H_2O)_7$		
Fe(1)–O(2)	2.093(4) × 2	Al(1)–O(1)/F(1)	1.867(3) × 2
Fe(1)–O(3)	2.105(3) × 2	Al(1)–F(2)	1.784(3) × 2
Fe(1)–O(4)	2.126(4) × 2	Al(1)–F(3)	1.787(2) × 2
Fe(2)–O(5)	2.087(4) × 2		
Fe(2)–O(6)	2.123(3) × 4		
H(1B) · · · O(2)	2.536 × 2	H(1B) · · · O(4)	2.267 × 2
H(2) · · · F(3)	1.732	H(3) · · · O(1)/F(1)	2.316
H(3) · · · F(2)	2.054	H(4) · · · O(1)/F(1)	1.963
H(5) · · · F(2)	1.729	H(6A) · · · F(2)	1.761
H(6A) · · · F(3)	1.704		
	$CoAlF_5(H_2O)_7$		
Co(1)–O(2)	2.045(4) × 2	Al(1)–O(1)/F(1)	1.863(3) × 2
Co(1)–O(3)	2.081(3) × 2	Al(1)–F(2)	1.779(2) × 2
Co(1)–O(4)	2.109(4) × 2	Al(1)–F(3)	1.786(2) × 2
Co(2)–O(5)	2.055(3) × 2		
Co(2)–O(6)	2.088(2) × 4		
H(1B) · · · O(2)	2.508 × 2	H(1B) · · · O(4)	2.172 × 2
H(2) · · · F(3)	1.716	H(3) · · · O(1)/F(1)	2.349
H(3) · · · F(2)	2.053	H(4) · · · O(1)/F(1)	1.949
H(5) · · · F(2)	1.731	H(6A) · · · F(2)	1.780
H(6A) · · · F(3)	1.718		
	$NiAlF_5(H_2O)_7$		
Ni(1)–O(2)	2.019(4) × 2	Al(1)–O(1)/F(1)	1.860(3) × 2
Ni(1)–O(3)	2.036(3) × 2	Al(1)–F(2)	1.775(3) × 2
Ni(1)–O(4)	2.079(4) × 2	Al(1)–F(3)	1.782(2) × 2
Ni(2)–O(5)	2.021(4) × 2		
Ni(2)–O(6)	2.057(3) × 4		
H(2) · · · F(3)	1.710	H(3) · · · O(1)/F(1)	2.291
H(3) · · · F(2)	2.114	H(4) · · · O(1)/F(1)	1.915
H(5) · · · F(2)	1.729	H(6A) · · · F(2)	1.783
H(6A) · · · F(3)	1.702		

Table 4. Selected bond distances for $M^{2+}AlF_5(H_2O)_7$ (M^{2+} = Fe^{2+}, Co^{2+}, or Ni^{2+}) at 100 K.

Bond	Distance (Å)	Bond	Distance (Å)
	$FeAlF_5(H_2O)_7$		
Fe(1)–O(3)	2.102(4) × 2	Al(1)–O(1)/F(1)	1.904(4) × 2
Fe(1)–O(4)	2.099(3) × 2	Al(1)–F(3)	1.769(4) × 2
Fe(1)–O(5)	2.138(4) × 2	Al(1)–F(4)	1.793(3) × 2
Fe(2)–O(6)	2.084(3) × 2	Al(2)–O(2)/F(2)	1.872(4) × 2
Fe(2)–O(7)	2.105(4) × 2	Al(2)–F(5)	1.794(3) × 2
Fe(2)–O(8)	2.138(4) × 2	Al(2)–F(6)	1.809(3) × 2
H(1A) · · · O(2)/F(2)	1.768 × 2	H(1B) · · · O(3)	2.270 × 2
H(1B) · · · O(5)	2.346 × 2	H(2A) · · · O(5)	1.814 × 2
H(2B) · · · O(1)/F(1)	1.789 × 2	H(3A) · · · O(2)/F(2)	2.639
H(3A) · · · O(5)	2.324	H(3B) · · · F(4)	1.713
H(4A) · · · O(1)/F(1)	1.824	H(4B) · · · O(2)/F(2)	2.652
H(4B) · · · F(6)	1.802	H(5A) · · · O(1)/F(1)	2.069
H(5B) · · · O(8)	1.964	H(6A) · · · F(3)	1.716
H(6B) · · · F(6)	1.769	H(7A) · · · F(4)	1.711
H(7B) · · · F(3)	1.740	H(8A) · · · F(6)	1.875
H(8B) · · · F(5)	1.680		
	$CoAlF_5(H_2O)_7$		
Co(1)–O(3)	2.055(3) × 2	Al(1)–O(1)/F(1)	1.892(3) × 2
Co(1)–O(4)	2.083(2) × 2	Al(1)–F(3)	1.776(2) × 2
Co(1)–O(5)	2.099(3) × 2	Al(1)–F(4)	1.788(2) × 2
Co(2)–O(6)	2.051(2) × 2	Al(2)–O(2)/F(2)	1.866(2) × 2
Co(2)–O(7)	2.081(3) × 2	Al(2)–F(5)	1.791(2) × 2
Co(2)–O(8)	2.085(3) × 2	Al(2)–F(6)	1.802(2) × 2
H(1A) · · · O(2)/F(2)	1.753 × 2	H(1B) · · · O(3)	2.267 × 2
H(2A) · · · O(5)	1.833 × 2	H(2B) · · · O(1)/F(1)	1.925 × 2
H(3A) · · · F(5)	1.713	H(3B) · · · F(4)	1.699
H(4A) · · · O(1)/F(1)	1.854	H(4B) · · · F(6)	1.793
H(5A) · · · O(1)/F(1)	2.046	H(5B) · · · O(7)	2.420
H(5B) · · · O(8)	2.083	H(6A) · · · F(3)	1.704
H(6B) · · · F(6)	1.755	H(7A) · · · F(4)	1.720
H(7B) · · · F(3)	1.762	H(8A) · · · F(6)	1.796
H(8B) · · · F(5)	1.690		
	$NiAlF_5(H_2O)_7$		
Ni(1)–O(3)	2.039(4) × 2	Al(1)–O(1)/F(1)	1.884(4) × 2
Ni(1)–O(4)	2.039(4) × 2	Al(1)–F(3)	1.793(4) × 2
Ni(1)–O(5)	2.064(4) × 2	Al(1)–F(4)	1.789(3) × 2
Ni(2)–O(6)	2.014(4) × 2	Al(2)–O(2)/F(2)	1.867(4) × 2
Ni(2)–O(7)	2.055(4) × 2	Al(2)–F(5)	1.789(3) × 2
Ni(2)–O(8)	2.058(4) × 2	Al(2)–F(6)	1.802(3) × 2
H(1B) · · · O(5)	2.031 × 2	H(2A) · · · O(5)	1.983 × 2
H(2B) · · · O(1)/F(1)	1.751 × 2	H(3A) · · · O(2)/F(2)	2.557
H(3A) · · · O(5)	2.351	H(3B) · · · F(4)	1.703
H(4A) · · · O(1)/F(1)	1.820	H(4B) · · · F(6)	1.806
H(5A) · · · O(1)/F(1)	2.110	H(5B) · · · O(7)	2.400
H(5B) · · · O(8)	2.024	H(6A) · · · F(3)	1.726
H(6B) · · · F(6)	1.742	H(7A) · · · F(4)	1.710
H(7B) · · · F(3)	1.817	H(8A) · · · F(6)	1.782
H(8B) · · · F(5)	1.687		

The powder X-ray diffraction (PXRD) data for $M^{2+}AlF_5(H_2O)_7$ (M^{2+} = Fe^{2+}, Co^{2+}, or Ni^{2+}) were collected using a PANalytical X'Pert pro diffractometer using CuKα radiation in the 2θ range of 5–65°. A step size of 0.008 degrees (deg) with a scan time of 0.3 s/deg was used. No impurities were observed, and the calculated and experimental PXRD patterns were in good agreement (see Supporting Information Figure S1).

Fourier-transform infrared spectroscopy (FT-IR) spectra of $M^{2+}AlF_5(H_2O)_7$ (M^{2+} = Fe^{2+}, Co^{2+}, or Ni^{2+}) were obtained using a Thermo Scientific Nicolet 6700 FT-IR spectrome-

ter in the range of 400–4000 cm^{-1}. Thermogravimetric analyses (TGA) for $M^{2+}AlF_5(H_2O)_7$ (M^{2+} = Fe^{2+}, Co^{2+}, or Ni^{2+}) were carried out using a TA Instruments TGA 2050. Approximately ~10 mg of each sample was placed into a Pt crucible and heated under a nitrogen atmosphere at a rate of 10 °C min^{-1} to 900 °C. The UV–Vis diffuse reflectance spectra of $M^{2+}AlF_5(H_2O)_7$ (M^{2+} = Fe^{2+}, Co^{2+}, or Ni^{2+}) were collected using a Shimadzu SolidSpec-3700 Diffuse Reflectance UV–VIS-NIR spectrophotometer in the range of 300–1400 nm.

3. Results and Discussion

3.1. Synthesis

Previously, various researchers reported the synthesis and crystal structures of mixed metal fluoride hydrates prepared via a hydrothermal method using HF as a mineralizer. For example, crystals of $Sr_2Fe_2F_{10}(H_2O)$ were prepared via a high-temperature (700 °C) hydrothermal method using an aqueous solution of SrF_2, Fe_2O_3, and HF [38]. Additionally, M(II)M'(III)$F_5(H_2O)_7$ (M = Co or Ni; M' = Mn, Ga, or In) were obtained via a hydrothermal method using an aqueous solution of $Co(NO_3)_2{\cdot}6H_2O$, $Ni(NO_3)_2{\cdot}6H_2O$, $Ga(NO_3)_3{\cdot}xH_2O$, $In(NO_3)_3{\cdot}xH_2O$, Mn_2O_3, $CoCO_3$, tetrapropylammoniumhydroxide (TPAOH), and HF at 170~200 °C [31].

However, HF is very toxic and corrosive, and it has a propensity to dissolve glass materials, posing serious health risks. Proper personal protective equipment and expertise in handling HF are essential. In a previous study, Kim et al. reported a new synthetic method to synthesize mixed metal fluorides using a CF_3COOH aqueous solution, providing a safer alternative [25]. Using this method, crystals of $M^{2+}AlF_5(H_2O)_7$ (M^{2+} = Fe^{2+}, Co^{2+}, or Ni^{2+}) can be easily and safely prepared without using an aqueous HF solution (see Figure 1). The hydrothermal conditions are believed to facilitate the in situ generation of aqueous HF from a CF_3COOH aqueous solution in the reaction mixture. The potential reaction mechanisms are as follows:

$$MF_2\ (s)\ (M^{2+} = Fe^{2+}, Co^{2+}, \text{or } Ni^{2+}) + AlF_3\ (s) + 5CF_3COOH\ (aq) \rightarrow (CF_3COO)_2M\ (aq)\ (M^{2+} = Fe^{2+}, Co^{2+}, \text{or } Ni^{2+}) + (CF_3COO)_3Al\ (aq) + 5HF\ (aq) \quad (1)$$

$$(CF_3COO)_2M\ (aq) + (CF_3COO)_3Al\ (aq) + 5HF\ (aq) \rightarrow M^{2+}AlF_5(H_2O)_7\ (s)\ (M^{2+} = Fe^{2+}, Co^{2+}, \text{or } Ni^{2+}) + 5CF_3H\ (g) + 5CO_2\ (g)\uparrow \quad (2)$$

Initially, the hydrothermal reaction of metal fluorides, $M^{2+}F_2$ (M^{2+} = Fe^{2+}, Co^{2+}, or Ni^{2+}) and AlF_3, with a CF_3COOH aqueous solution led to the in situ generation of metal trifluoroacetate salts and aqueous HF. Subsequently, the in situ intermediates are expected to further reactions, ultimately resulting in the formation of $M^{2+}AlF_5(H_2O)_7$ (M^{2+} = Fe^{2+}, Co^{2+}, or Ni^{2+}).

3.2. Crystal Structure

The crystal structures of $M^{2+}AlF_5(H_2O)_7$ (M^{2+} = Fe^{2+}, Co^{2+}, or Ni^{2+}) exhibit both $C2/m$ (No. 12) or P-1 (No. 2) space groups depending on the temperature (see Table 2). At room temperature, $M^{2+}AlF_5(H_2O)_7$ (M^{2+} = Fe^{2+}, Co^{2+}, or Ni^{2+}) reveals a zero-dimensional structure. Two crystallographically unique M^{2+} sites give rise to octahedral hexa-aqua complexes, $[M(H_2O)_6]^{2+}$ (M^{2+} = Fe^{2+}, Co^{2+}, or Ni^{2+}) alongside octahedral $[AlF_5(H_2O)]^{2-}$ complexes, where O and F atoms are disordered (see Figure 2). These cationic and anionic complexes, $[M(H_2O)_6]^{2+}$ (M^{2+} = Fe^{2+}, Co^{2+}, or Ni^{2+}) and $[AlF_5(H_2O)]^{2-}$, are interconnected through hydrogen bonding, as illustrated in Figure 3. Thus, it exhibits a *pseudo* ABAB layered structure along the b-axis. The corresponding hydrogen bonding distances between H and O or O/F vary from 1.702 to 2.536 Å (see Table 2). In addition, the M^{2+} (M^{2+} = Fe^{2+}, Co^{2+}, or Ni^{2+}) – O bond distances in the octahedral complexes of $[M(H_2O)_6]^{2+}$ range between 2.021(4) and 2.126(4) Å, and the Al–F or O/F bond distances of the $[AlF_5(H_2O)]^{2-}$ complex range from 1.775(3) to 1.867(3) Å, respectively. Selected bond distances for $M^{2+}AlF_5(H_2O)_7$ (M^{2+} = Fe^{2+}, Co^{2+}, or Ni^{2+}) at RT are also summarized in Table 3. The bond valence sum (BVS) [39,40] calculations resulted in values of 2.05~2.06,

2.08, 2.09, 3.06~3.12, 1.64~2.01, and 0.85~1.10 for Fe^{2+}, Co^{2+}, Ni^{2+}, Al^{3+}, O^{2-}, and F^{-}, respectively (see Supporting Information Table S3).

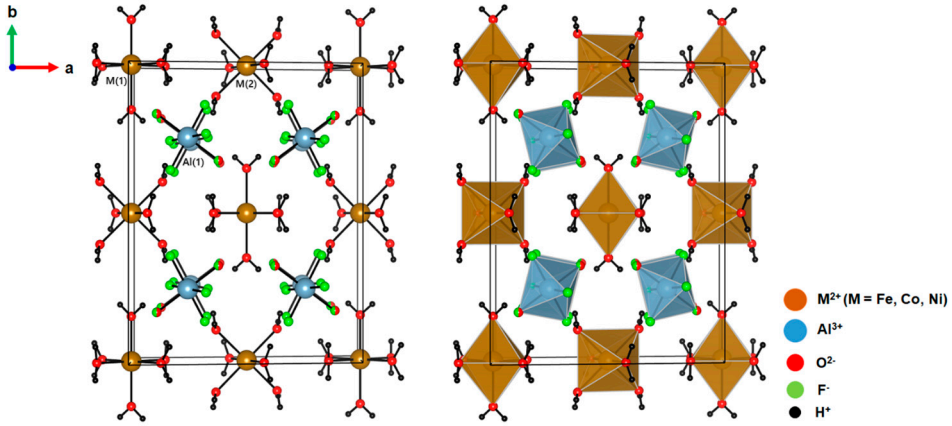


Figure 2. Ball-and-stick and polyhedral representations of $M^{2+}AlF_5(H_2O)_7$ (M^{2+} = Fe^{2+}, Co^{2+}, or Ni^{2+}) at room temperature in the *ab*-plane. Octahedral complexes, $[M(H_2O)_6]^{2+}$ and $[AlF_5(H_2O)]^{2-}$, are balanced by electrostatic charges. Hydrogen atoms bonded to disordered O/F sites were excluded to enhance clarity.

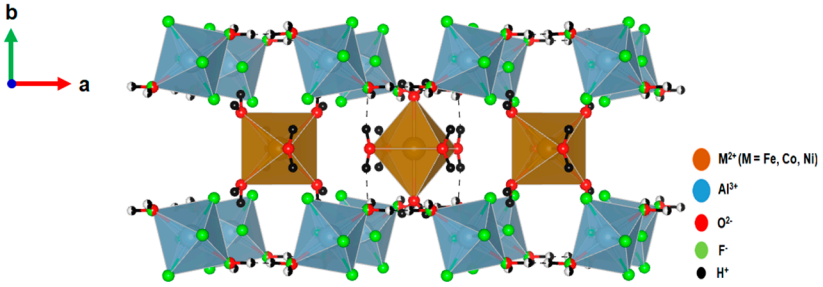


Figure 3. Hydrogen bonding interactions between two structural components, $[M(H_2O)_6]^{2+}$ and $[AlF_5(H_2O)]^{2-}$ within the $M^{2+}AlF_5(H_2O)_7$ (M^{2+} = Fe^{2+}, Co^{2+}, or Ni^{2+}) at room temperature. Hydrogen bonding interactions produce a *pseudo* ABAB layered structure.

Similar to the room temperature structure, $M^{2+}AlF_5(H_2O)_7$ (M^{2+} = Fe^{2+}, Co^{2+}, or Ni^{2+}) at 100(2) K adopts a zero-dimensional structure (see Figure 4). This structure features two distinct octahedral cations, $[M(H_2O)_6]^{2+}$ and two distinct octahedral anions, $[AlF_5(H_2O)]^{2-}$, with disorder observed in the positioning of both O and F atoms. These different components bind to each other through hydrogen bonding and electrostatic interactions, contributing to a *pseudo* ABAB layered structure, as illustrated in Figure 5. The corresponding hydrogen bonding distances between H and O or O/F vary from 1.680 to 2.639 Å. The M^{2+}–O bond distances in the octahedral $[M(H_2O)_6]^{2+}$ complexes range from 2.014(4) to 2.138(4) Å, and the Al–F or O/F bond distances in the octahedral $[AlF_5(H_2O)]^{2-}$ complexes range from 1.769(4) to 1.904(4) Å, respectively. Selected bond distances for $M^{2+}AlF_5(H_2O)_7$ (M^{2+} = Fe^{2+}, Co^{2+}, or Ni^{2+}) at 100 K are summarized in Table 4. The BVS [39,40] calculations resulted in values of 2.04~2.06, 2.07~2.11, 2.07~2.10, 2.96~3.02, 1.63~1.97, and 0.69~1.24 for Fe^{2+}, Co^{2+}, Ni^{2+}, Al^{3+}, O^{2-}, and F^{-}, respectively (see Supporting Information Table S3).

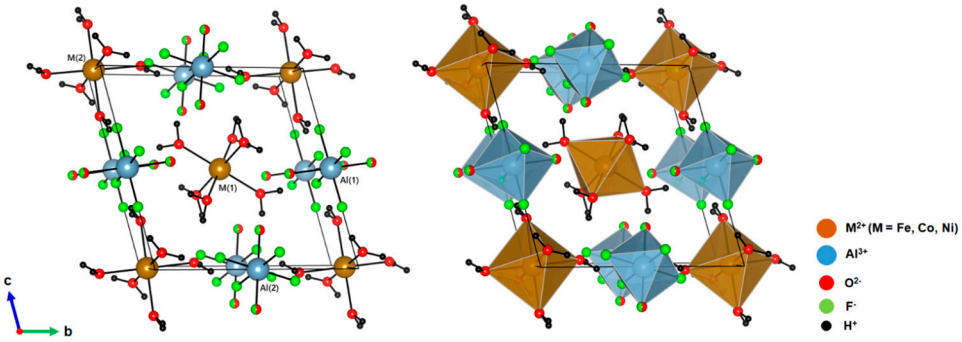


Figure 4. Ball-and-stick and polyhedral representations of $M^{2+}AlF_5(H_2O)_7$ (M^{2+} = Fe^{2+}, Co^{2+}, or Ni^{2+}) at 100 K in the *bc*-plane. Electrostatic charges are balanced between octahedral complexes, $[M(H_2O)_6]^{2+}$ and $[AlF_5(H_2O)]^{2-}$. Hydrogen atoms bonded to disordered O/F sites were excluded to enhance clarity.

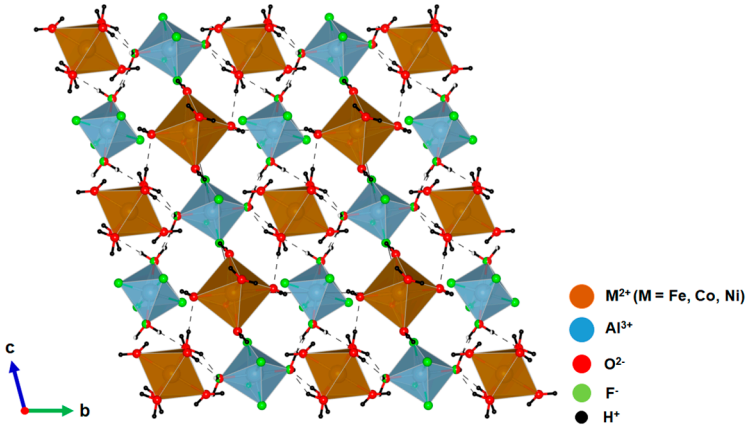


Figure 5. Polyhedral representations of hydrogen bonding interactions between $[M(H_2O)_6]^{2+}$ and $[AlF_5(H_2O)]^{2-}$ within the $M^{2+}AlF_5(H_2O)_7$ (M^{2+} = Fe^{2+}, Co^{2+}, or Ni^{2+}) at 100 K in the *bc*-plane. A *pseudo* ABAB layered structure in the *bc*-plane is shown with hydrogen bonds.

The observed polymorphism in $M^{2+}AlF_5(H_2O)_7$ (M^{2+} = Fe^{2+}, Co^{2+}, or Ni^{2+}) is associated with alternations in the local coordination environment of $[M(H_2O)_6]^{2+}$ and $[AlF_5(H_2O)]^{2-}$ octahedra, accompanied by changes in the M^{2+}–O (M^{2+} = Fe^{2+}, Co^{2+}, or Ni^{2+}) and Al^{3+}–F or O/F bond lengths. Despite the expected tilting of these octahedra, indicative of out-of-center distortion in octahedral structures, such effects were not discernible in $M^{2+}AlF_5(H_2O)_7$ (see Supporting Information, Table S4). Initially, as the temperature decreased, the unit cell volume reduced by approximately 2.03 times. This led to increased strength in hydrogen bonding interactions between $[M(H_2O)_6]^{2+}$ and $[AlF_5(H_2O)]^{2-}$ octahedra, accompanied by an augmentation in the number of hydrogen bonds. Furthermore, the local coordination environments of $[M(H_2O)_6]^{2+}$ and $[AlF_5(H_2O)]^{2-}$ exhibited subtle changes with temperature variations. For instance, the average bond distances of Fe–O in the axial position of $[Fe(H_2O)_6]^{2+}$ increased as the temperature decreased (see Figure 6). Additionally, the number of crystallographic Al sites increases to two under ~100 K temperature conditions. In summary, this led to reduced crystal symmetry, ultimately inducing a polymorphism between monoclinic *C*2/*m* (No. 12) and triclinic *P*-1 (No. 2).

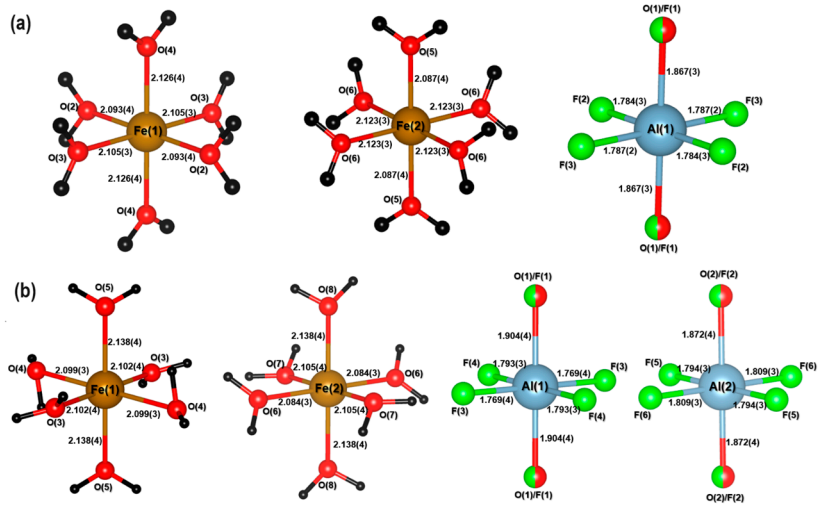


Figure 6. Ball-and-stick representations of the local coordination environments of $[Fe(H_2O)_6]^{2+}$ and $[AlF_5(H_2O)]^{2-}$ within $FeAlF_5(H_2O)_7$ at two different temperatures: (**a**) room temperature and (**b**) 100 K.

3.3. FT-IR Spectroscopy

The FT-IR spectra of $M^{2+}AlF_5(H_2O)_7$ (M^{2+} = Fe^{2+}, Co^{2+}, or Ni^{2+}) revealed distinctive O–H vibrations around 3400 cm^{-1} and 1650 cm^{-1}, attributed to the presence of water molecules [41]. The bands occurring between 730–700 cm^{-1} and 670–450 cm^{-1} can be assigned to Al–F or Al–O/F and M^{2+}–O (M^{2+} = Fe^{2+}, Co^{2+}, or Ni^{2+}) vibrations, respectively. These assignments are consistent with previous reported results [41]. Detailed IR spectra and corresponding assignments are provided in the Supporting Information (see Figure S3).

3.4. Thermal Analysis

The thermal behavior of $M^{2+}AlF_5(H_2O)_7$ (M^{2+} = Fe^{2+}, Co^{2+}, or Ni^{2+}) was investigated using a thermogravimetric analysis (TGA) under a nitrogen atmosphere. All three materials exhibited two distinct weight loss steps (see Figure 7 and Table 5).

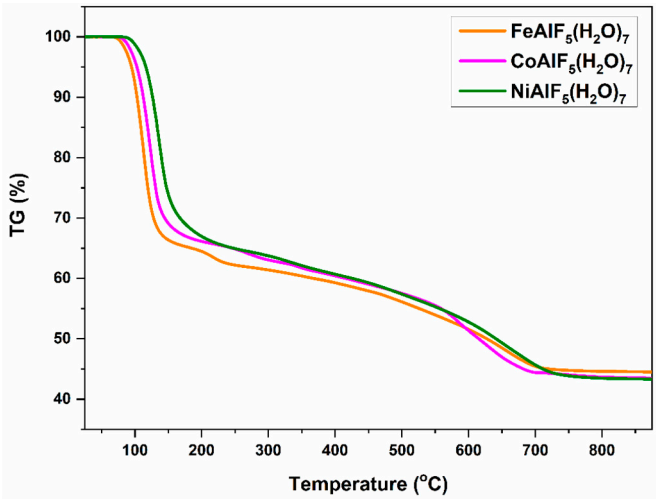


Figure 7. Thermogravimetric analysis (TGA) diagrams for $M^{2+}AlF_5(H_2O)_7$ (M^{2+} = Fe^{2+}, Co^{2+}, or Ni^{2+}).

Table 5. Weight loss% of $M^{2+}AlF_5(H_2O)_7$ (M^{2+} = Fe^{2+}, Co^{2+}, or Ni^{2+}).

Sample	[a] First Weight Loss% (Found, Calculated)	[b] Final Weight Loss% (Found)
$FeAlF_5(H_2O)_7$	35.6, 35.6	55.3
$CoAlF_5(H_2O)_7$	34.1, 35.2	56.3
$NiAlF_5(H_2O)_7$	34.1, 35.2	56.5

[a] Released six water molecules ($-6H_2O$). [b] The composition of the residue for samples, determined using XRD.

For $FeAlF_5(H_2O)_7$, the initial weight loss (found: ~35.6%) observed between 100 °C and 200 °C can be attributed to the release of six coordinated water molecules from the crystal structure (calculated: 35.6%). Subsequently, a second weight loss between 200 °C and 800 °C is expected due to the sample decomposition (found: ~55.3%). The powder XRD pattern of the final residue product after TGA revealed the presence of Fe_2O_3 and unidentified phases (possibly Al_2O_3 or $AlFeO_3$, etc.) (see Supporting information, Figure S4).

In the case of $CoAlF_5(H_2O)_7$, the initial weight loss (found: ~34.10%) that occurred between 100 °C and 220 °C corresponded to the release of six water molecules from the crystal structure (calculated: 35.2%). A subsequent weight loss between 200 °C and 800 °C suggested the occurrence of sample decomposition (found: ~56.3%). The powder XRD pattern of the final residue product after TGA displayed the formation of $CoAl_2O_4$ (see Supporting Information, Figure S4).

For $NiAlF_5(H_2O)_7$, the initial weight loss (found: ~34.07%) observed between 100 °C and 220 °C was attributed to the release of six water molecules from the crystal structure (calculated: 35.2%). A subsequent weight loss between 200 °C and 800 °C was indicative of sample decomposition (found: ~56.5%). The powder XRD pattern of the final residue product after TGA showed the presence of NiO and $NiAl_2O_4$ (see Supporting Information, Figure S4).

It is noteworthy that a prior TGA investigation focused on specific $M^{2+}M'^{3+}F_5(H_2O)_7$ materials revealed the existence of dihydrate intermediates, namely $M^{2+}M'^{3+}F_5(H_2O)_2$, with an inverse weberite structure. These intermediates have been successfully isolated or synthesized in previous studies [42,43]. However, in the current study, we were unable to isolate such intermediates. Indeed, the ability to obtain these intermediates may be influenced by the specific chemical compositions and crystal structures of $M^{2+}M'^{3+}F_5(H_2O)_7$.

3.5. UV–Vis Diffuse Reflectance Spectroscopy

UV–vis diffuse reflectance spectra of $M^{2+}AlF_5(H_2O)_7$ (M^{2+} = Fe^{2+}, Co^{2+}, or Ni^{2+}) in the range of 300–1400 nm are presented in Figure 8. Notably, the crystal structure of all three materials contains $[M(H_2O)_6]^{2+}$ (M^{2+} = Fe^{2+}, Co^{2+}, or Ni^{2+}) complexes, implying the anticipated appearance of distinct absorption bands for each material (see Figure 8).

For $FeAlF_5(H_2O)_7$, absorption with two broad peaks between 800 nm and 1300 nm was observed, corresponding to the $^5T_2 \rightarrow {}^5E$ transition. The splitting of this absorption band is attributed to the Jahn–Teller distortion of the excited state $t_{2g}{}^3e_g{}^3$ in Fe^{2+} (d^6) [44,45].

In the case of $CoAlF_5(H_2O)_7$, the broad band near 500 nm can be attributed to the $^4T_{1g}$ (F) $\rightarrow {}^4T_{1g}$ (P) transition, and a slightly higher energy transition (the shoulder) is predicted to be the $^4T_{1g} \rightarrow {}^4A_{2g}$ transition. The small energy difference results in the overlap of these two bands. Additionally, a broad band near 1200 nm was observed, assigned as the $^4T_{1g} \rightarrow {}^4T_{2g}$ transition [44,45].

For $NiAlF_5(H_2O)_7$, three principal absorption bands were identified, with one of the bands exhibiting signs of further splitting. The band near 400 nm was assigned to the $^3A_{2g} \rightarrow {}^3T_{1g}$(P) transition. A two-humped absorption band near 700 nm was assigned to the spin-forbidden $^3A_{2g} \rightarrow {}^1E_g$ transition (~620 nm, weak) and the $^3A_{2g} \rightarrow {}^3T_{1g}$(F) transition (~725 nm), respectively. The splitting of these bands was a result of Jahn–Teller distortion in the excited state. The last band near 1200 nm was assigned to the $^3A_{2g} \rightarrow {}^3T_{2g}$ transition [44,45].

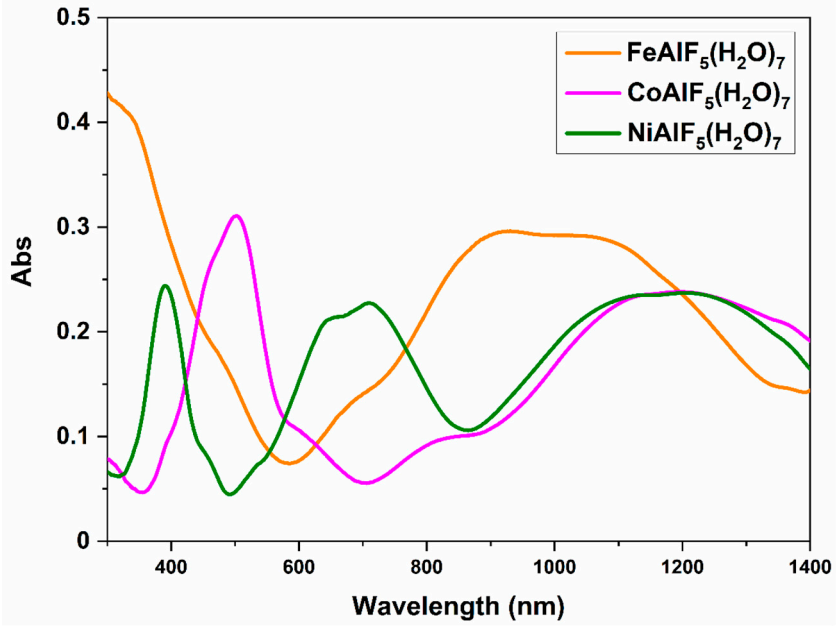


Figure 8. UV–Vis diffuse reflectance spectra of $M^{2+}AlF_5(H_2O)_7$ (M^{2+} = Fe^{2+}, Co^{2+}, or Ni^{2+}).

4. Conclusions

The synthesis and characterization of three novel mixed metal fluorides hydrates, $M^{2+}AlF_5(H_2O)_7$ (M^{2+} = Fe^{2+}, Co^{2+}, or Ni^{2+}), have been successfully achieved using a hydrothermal method employing a CF_3COOH aqueous solution. The crystal structures exhibited polymorphisms in $C2/m$ (No. 12) or P-1 (No. 2) space groups, with these polymorphisms linked to variations in the local environment of $[M(H_2O)_6]^{2+}$ and $[AlF_5(H_2O)]^{2-}$ octahedra in response to temperature changes. The presence of water molecules in the synthesized materials was confirmed through FT-IR and TGA analyses, highlighting the significance of hydration in the structural framework. UV–Vis spectra of $M^{2+}AlF_5(H_2O)_7$ (M^{2+} = Fe^{2+}, Co^{2+}, or Ni^{2+}) showed a distinctive absorption band, dependent on the $[M(H_2O)_6]^{2+}$ complex, providing valuable insights into the electronic transition within the material.

This comprehensive study not only contributes to the understanding of the synthetic procedure and crystal structures of $M^{2+}AlF_5(H_2O)_7$ (M^{2+} = Fe^{2+}, Co^{2+}, or Ni^{2+}) but also sheds light on the intricate relationship between the two polymorphs and the evolving coordination environments of the M^{2+} and Al^{3+} cations. The presented findings provide a robust exploration and applications of mixed metal fluoride hydrates in the field of material sciences.

Supplementary Materials: The following supporting information can be downloaded at: https://www.mdpi.com/article/10.3390/cryst14020197/s1, Table S1: Atomic coordinates and equivalent isotropic displacement parameters (Å^2) for $M^{2+}AlF_5(H_2O)_7$ (M^{2+} = Fe^{2+}, Co^{2+}, or Ni^{2+}) at RT. Table S2: Atomic coordinates and equivalent isotropic displacement parameters (Å^2) for $M^{2+}AlF_5(H_2O)_7$ (M^{2+} = Fe^{2+}, Co^{2+}, or Ni^{2+}) at 100 K. Table S3: Bond valence calculation for $M^{2+}AlF_5(H_2O)_7$ (M^{2+} = Fe^{2+}, Co^{2+}, or Ni^{2+}) at RT and 100 K, respectively. Table S4: Out-of-center distortion of octahedral structures in $[Fe(H_2O)_6]^{2+}$ at RT and 100 K. Figure S1: Experimental and calculated X-ray powder diffraction patterns for $M^{2+}AlF_5(H_2O)_7$ (M^{2+} = Fe^{2+}, Co^{2+}, or Ni^{2+}): (a) $FeAlF_5(H_2O)_7$, (b) $CoAlF_5(H_2O)_7$, and (c) $NiAlF_5(H_2O)$. Figure S2: ORTEP representation (50% probability ellipsoid) for $M^{2+}AlF_5(H_2O)_7$ (M^{2+} = Fe^{2+}, Co^{2+}, or Ni^{2+}). Figure S3: FT-IR Spectra of $M^{2+}AlF_5(H_2O)_7$ (M^{2+} = Fe^{2+}, Co^{2+}, or Ni^{2+}): (a) $FeAlF_5(H_2O)_7$, (b) $CoAlF_5(H_2O)_7$, and (c) $NiAlF_5(H_2O)_7$. Figure S4: Powder X-ray diffraction pattern for final residuals after TGA experiments: (a) $FeAlF_5(H_2O)_7$, (b) $CoAlF_5(H_2O)_7$, and (c) $NiAlF_5(H_2O)_7$.

Author Contributions: Conceptualization, J.M.S. and S.W.K.; validation, J.M.S., H.J., M.H.C., K.M.O., H.Y.C., and S.W.K.; formal analysis, J.M.S., H.J., M.H.C., K.M.O., H.Y.C., and S.W.K.; investigation,

J.M.S., H.J., M.H.C., K.M.O., H.Y.C., and S.W.K.; data curation, J.M.S., H.J., M.H.C., K.M.O., H.Y.C., and S.W.K.; writing—original draft preparation, J.M.S. and S.W.K.; writing—review and editing, J.M.S., H.J., M.H.C., K.M.O., H.Y.C., and S.W.K.; visualization, J.M.S. and S.W.K.; supervision, S.W.K.; project administration, S.W.K.; funding acquisition, S.W.K. All authors have read and agreed to the published version of the manuscript.

Funding: This research received funding from the National Research Foundation of Korea (NRF), Ministry of Education (2022R111A3063132). H.Y.C. also thanks the Robert A. Welch Foundation for support (Gant AK-0050-20201025).

Data Availability Statement: The corresponding crystallographic information files (CIFs) have been deposited in the Cambridge Crystallographic Centre (CCDC) database and can be obtained free of charge at: http://www.ccdc.cam.ac.uk/conts/retrieving.html (accessed on 22 January 2024) (or from the CCDC, 12 Union Road, Cambridge CB2 1EZ, UK; Fax: +44-1223-336033; E-mail: deposit@ccdc.cam.ac.uk) with the following depository number: 2327066~2327071. The data presented in this study are available from the corresponding author upon request. The data are not publicly available due to privacy.

Conflicts of Interest: The authors declare no conflicts of interest.

References

1. Leblanc, M.; Maisonneuve, V.; Tressaud, A. Crystal Chemistry and Selected Physical Properties of Inorganic Fluorides and Oxide-Fluorides. *Chem. Rev.* **2015**, *115*, 1191–1254. [CrossRef]
2. Yu, Y.; Liu, R.; Zhao, H.; Xu, Y.; Xu, B.; Li, Q.; Du, J.; Xu, Q. Room temperature multiferroic $BaMnF_4$ films. *J. Magn. Magn. Mater.* **2020**, *494*, 165782. [CrossRef]
3. Poole, A.; Roessli, B.; Zaharko, O.; Kramer, K.W. The magnetic structure of multiferroic $BaMnF_4$. *J. Phys.-Condes. Matter* **2011**, *23*, 266004. [CrossRef]
4. Keve, E.T.; Abrahams, S.C.; Bernstein, J.L. Crystal structure of pyroelectric paramagnetic barium manganese fluoride, $BaMnF_4$. *J. Chem. Phys.* **1969**, *51*, 4928–4936. [CrossRef]
5. Zhou, S.; Dai, C.; Xu, Q.; Du, J. The magnetic properties of multiferroic $BaCoF_4$. *AIP Adv.* **2017**, *7*, 055822. [CrossRef]
6. Borisov, P.; Johnson, T.A.; García-Castro, A.C.; Kc, A.; Schrecongost, D.; Cen, C.; Romero, A.H.; Lederman, D. Multiferroic $BaCoF_4$ in Thin Film Form: Ferroelectricity, Magnetic Ordering, and Strain. *ACS Appl. Mater. Interfaces.* **2016**, *8*, 2694–2703. [CrossRef] [PubMed]
7. Keve, E.T.; Abrahams, S.C.; Bernstein, J.L. Ferroelectric paraelastic paramagnetic barium cobalt fluoride, $BaCoF_4$, crystal structure. *J. Chem. Phys.* **1970**, *53*, 3279–3287. [CrossRef]
8. Xu, Q.; Dai, C.; Wang, J.; Li, C.; Li, Q.; Du, J. Enhanced ferromagnetism in $BaNiF_4$ film. *J. Alloys Comp.* **2018**, *741*, 265–268. [CrossRef]
9. Ederer, C.; Spaldin, N.A. Electric-field-switchable magnets: The case of $BaNiF_4$. *Phys. Rev. B* **2006**, *74*, 020401. [CrossRef]
10. Mezzadri, F.; Calestani, G.; Pernechele, C.; Solzi, M.; Spina, G.; Cianchi, L.; Del, G.F.; Lantieri, M.; Buzzi, M.; Gilioli, E. Magnetic and Mossbauer characterization of the multiferroic fluoride $K_3Fe_5F_{15}$. *Phys. Rev. B* **2011**, *84*, 104418. [CrossRef]
11. Blinc, R.; Tavcar, G.; Zemva, B.; Hanzel, D.; Cevc, P.; Filipic, C.; Levstik, A.; Jaglicic, Z.; Trontelj, Z.; Dalal, N.; et al. Weak ferromagnetism and ferroelectricity in $K_3Fe_5F_{15}$. *J. Appl. Phys.* **2008**, *103*, 074114. [CrossRef]
12. Ravez, J.; Abrahams, S.C.; de Pape, R. Ferroelectric-ferroelastic properties of potassium iron fluoride ($K_3Fe_5F_{15}$) and the phase transition at 490 K. *J. Appl. Phys.* **1989**, *65*, 3987–3990. [CrossRef]
13. Jaglicic, Z.; Pajic, D.; Trontelj, Z.; Dolinsek, J.; Jagodic, M. Magnetic memory effect in multiferroic $K_3Fe_5F_{15}$ and $K_3Cr_2Fe_3F_{15}$. *Appl. Phys. Lett.* **2013**, *102*, 242410. [CrossRef]
14. Blinc, R.; Cevc, P.; Potočnik, A.; Žemva, B.; Goreshnik, E.; Hanžel, D.; Gregorovič, A.; Trontelj, Z.; Jagličič, Z.; Laguta, V.; et al. Magnetic properties of multiferroic $K_3Cr_2Fe_3F_{15}$. *J. Appl. Phys.* **2010**, *107*, 043511. [CrossRef]
15. Blinc, R.; Cevc, P.; Tavčar, G.; Žemva, B.; Laguta, V.; Trontelj, Z.; Jagodič, M.; Pajić, D.; Balčytis, A.; Scott, J.F. Magnetism in multiferroic $Pb_5Cr_3F_{19}$. *Phys. Rev. B* **2012**, *85*, 054419. [CrossRef]
16. Andriamampianina, V.; Gravereau, P.; Ravez, J.; Abrahams, S.C. Relationship between the structures of ferroelectric $Pb_5Cr_3F_{19}$ and antiferroelectric $Pb_5Al_3F_{19}$ at 295 K and the phase III-phase IV transition in $Pb_5Al_3F_{19}$ on cooling to about 110 K. *Acta Cryst. B* **1994**, *50*, 135–141. [CrossRef]
17. Mateos, L.; Ramírez, M.O.; Carrasco, I.; Molina, P.; Galisteo-López, J.F.; Víllora, E.G.; de las Heras, C.; Shimamura, K.; Lopez, C.; Bausá, L.E. $BaMgF_4$: An Ultra-Transparent Two-Dimensional Nonlinear Photonic Crystal with Strong $\chi^{(3)}$ Response in the UV Spectral Region. *Adv. Funct. Mater.* **2014**, *24*, 1509–1518. [CrossRef]
18. Bergman, J.G.; Crane, G.R.; Guggenheim, H. Linear and nonlinear optical properties of ferroelectric barium magnesium fluoride ($BaMgF_4$) and barium zinc fluoride ($BaZnF_4$). *J. Appl. Phys.* **1975**, *46*, 4645–4646. [CrossRef]
19. Lian, X.; Yao, W.-D.; Liu, W.; Tang, R.-L.; Guo, S.-P. KNa_2ZrF_7: A Mixed-Metal Fluoride Exhibits Phase-Matchable Second-Harmonic-Generation Effect and High Laser-Induced Damage Threshold. *Inorg. Chem.* **2021**, *60*, 19–23. [CrossRef]

20. Tang, R.-L.; Lian, X.; Li, X.-H.; Huai, L.; Liu, W.; Guo, S.-P. From $CsKTaF_7$ to $CsNaTaF_7$: Alkali Metal Cations Regulation to Generate SHG Activity. *Chem. Eur. J.* **2022**, *28*, e202201588. [CrossRef]
21. Kavand, A.; Serra, C.A.; Blanck, C.; Lenertz, M.; Anton, N.; Vandamme, T.F.; Mély, Y.; Przybilla, F.; Chan-Seng, D. Controlled Synthesis of $NaYF_4$:Yb,Er Upconversion Nanocrystals as Potential Probe for Bioimaging: A Focus on Heat Treatment. *ACS Appl. Nano Mater.* **2021**, *4*, 5319–5329. [CrossRef]
22. Qiang, J.; Ruan, H.; Wang, L.; Wang, T.; Lei, J.; Liao, S.; Li, S. Luminescence Enhancement of K_2LiAlF_6:Mn^{4+} Phosphors by Zn^{2+}-Mediated Charge Compensation for Fast-Response Backlighting Applications. *Inorg. Chem.* **2023**, *62*, 14344–14354. [CrossRef] [PubMed]
23. Yang, J.; Wu, H.; Song, L.; Wang, X.; Dong, J.; Gan, S.; Zou, L. A novel synthesis route to monodisperse $Na_5Lu_9F_{32}$:Tb^{3+} phosphors with superior thermal stability. *J. Lumin.* **2018**, *204*, 533–538. [CrossRef]
24. Hagenmuller, P. *INORGANIC SOLID FLUORIDES Chemistry and Physics*; Academic Press, Inc.: Orlando, FL, USA, 1985.
25. Kim, S.W.; Chang, H.Y.; Halasyamani, P.S. Selective Pure-Phase Synthesis of the Multiferroic $BaMF_4$ (M = Mg, Mn, Co, Ni, and Zn) Family. *J. Am. Chem. Soc.* **2010**, *132*, 17684–17685. [CrossRef]
26. Kim, S.W.; Kim, S.-H.; Halasyamani, P.S.; Green, M.A.; Bhatti, K.P.; Leighton, C.; Das, H.; Fennie, C.J. $RbFe^{2+}Fe^{3+}F_6$: Synthesis, structure, and characterization of a new charge-ordered magnetically frustrated pyrochlore-related mixed-metal fluoride. *Chem. Sci.* **2012**, *3*, 741–751. [CrossRef]
27. Kim, S.W.; Zhang, R.; Halasyamani, P.S.; Hayward, M.A. $K_4Fe_3F_{12}$: An Fe^{2+}/Fe^{3+} Charge-Ordered, Ferrimagnetic Fluoride with a Cation-Deficient, Layered Perovskite Structure. *Inorg. Chem.* **2015**, *54*, 6647–6652. [CrossRef] [PubMed]
28. Herdtweck, E.; Massa, W. Die Struktur der Fluoridhydrate $CoAlF_5 \cdot 7H_2O$ und $MnFeF_5 \cdot 7H_2O$. *Z. Anorg. Allg. Chem.* **1989**, *579*, 191–199. [CrossRef]
29. Davidovich, R.L.; Udovenko, A.A.; Logvinova, V.B.; Tkachev, V.V.; Shilov, G.V.; Kaidalova, T.A. Single Crystal X-ray Diffraction Study of Indium(III) and Gallium(III) Fluoride Complexes $M^{II}AF_5 \cdot 7H_2O$ (M = Co, Ni, Cu, Zn, Cd; A = In, Ga). *J. Struct. Chem.* **2018**, *59*, 1400–1404. [CrossRef]
30. Felder, J.B.; Smith, M.D.; Sefat, A.; zur Loye, H.-C. Magnetic and thermal behavior of a family of compositionally related zero-dimensional fluorides. *Solid State Sci.* **2018**, *81*, 19–25. [CrossRef]
31. Keerthisinghe, N.; Klepov, V.V.; Zhang, E.; Smith, M.D.; Egodawatte, S.; Foulger, S.H.; zur Loye, H.-C. Hydrothermal synthesis and properties of $M^{II}M^{III}F_5(H_2O)_7$ (M^{II} = Co^{2+} and Ni^{2+}, M^{III} = Mn^{3+}, Ga^{3+}, and In^{3+}). *Solid State Sci.* **2020**, *108*, 106374. [CrossRef]
32. *SAINT, Program for Area Detector Absorption Correction, 4.05*; Siemens Analytical X-ray Systems: Madison, WI, USA, 1995.
33. de la Flor, G.; Kroumova, E.; Hanson, R.M.; Aroyo, M.I. The International Tables Symmetry Database. *J. Appl. Crystallogr.* **2023**, *56*, 1824–1840. [CrossRef]
34. Sheldrick, G.M. SHELXT—Integrated space-group and crystal-structure determination. *Acta Crystallogr. Sect. A Found. Adv.* **2015**, *71*, 3–8. [CrossRef] [PubMed]
35. Sheldrick, G.M. Crystal structure refinement with SHELXL. *Acta Crystallogr. Sect. C Struct. Chem.* **2015**, *71*, 3–8. [CrossRef] [PubMed]
36. Farrugia, L.J. WinGX and ORTEP for Windows: An update. *J. Appl. Crystallogr.* **2012**, *45*, 849–854. [CrossRef]
37. Momma, K.; Izumi, F. VESTA: A three-dimensional visualization system for electronic and structural analysis. *J. Appl. Crystallogr.* **2008**, *41*, 653–658. [CrossRef]
38. Le Meins, J.-M.; Hemon-Ribaud, A.; Courbion, G. $Sr_2Fe_2F_{10}.H_2O$, the first hydrated strontium iron(III) fluoride. *Acta Crystallogr. Sect. C Cryst. Struct. Commun.* **1997**, *C53*, 1165–1166. [CrossRef]
39. Brown, I.D. *The Chemical Bond in Inorganic Chemistry: The Bond Valence Model*, 1st ed.; Oxford University Press: Oxford, UK, 2002.
40. Brown, I.D. Recent developments in the methods and applications of the Bond Valence Model. *Chem. Rev.* **2009**, *109*, 6858–6919. [CrossRef]
41. Nakamoto, K. *Infrared and Raman Spectra of Inorganic and Coordination Compounds Part A: Theory and Applications in Inorganic Chemistry*, 5th ed.; John Wiley & Sons, Inc.: New York, NY, USA, 1997.
42. Gallagher, K.J.; Ottaway, M.R. Mixed-metal fluoride hydrates and their thermal-decomposition products: An investigation by X-ray, Mössbauer, and thermal analysis. *J. Chem. Soc. Dalton Trans.* **1977**, 2212–2219. [CrossRef]
43. Keerthisinghe, N.; Berseneva, A.A.; Klepov, V.V.; Morrison, G.; zur Loye, H.-C. A Geometrically Frustrated Family of $M^{II}M^{III}F_5(H_2O)_2$ Mixed–Metal Fluorides with Complex Magnetic Interactions. *Inorg. Chem.* **2021**, *60*, 14318–14329. [CrossRef]
44. Surhone, L.M.; Tennoe, M.T.; Henssonow, S.F. *Tanabe-Sugano Diagram*; Betascript Publishing: Beau Bassin, Mauritius, 2011.
45. Miessler, G.L.; Fischer, P.J.; Tarr, D.A. *Inorganic Chemistry*; Pearson Education: Beijing, China, 2013.

Disclaimer/Publisher's Note: The statements, opinions and data contained in all publications are solely those of the individual author(s) and contributor(s) and not of MDPI and/or the editor(s). MDPI and/or the editor(s) disclaim responsibility for any injury to people or property resulting from any ideas, methods, instructions or products referred to in the content.